Molecules Designed to Contain Two Weakly Coupled Spins with a Photo-switchable Spacer

Jorge Salinas Uber,[a] Marta Estrader,[a] Jordi Garcia,[a] Paul Lloyd-Williams,[a] Anna Sadurní,[a] Dominik Dengler,[b] Joris van Slageren,[b] Nicholas F. Chilton,[c] Olivier Roubeau,[d],* Simon J. Teat,[e] Jordi Ribas-Ariño,[f] and Guillem Aromí.[a,g],*

Abstract: Controlling the charges and spins of molecules lies at the heart of spintronics. We report the design of a photoswitchable molecule consisting of two independent spins separated by a photo-switchable moiety contained within a new ligand, H_4L, that features a dithienylethene photochromic unit and two lateral coordinating moieties, yielding molecules with the [MM···MM] topology. Compounds $[M_4L_2(py)_6]$ (M = Cu, **1**; Co, **2**; Ni, **3**; Zn, **4**) have been prepared and described by single crystal X-ray diffraction (SCXRD). The structure allows different metals to be selectively distributed amongst the two chemically distinct sites of the ligand, enabling the preparation of many double-spin systems. Heterometallic [MM'···M'M] analogues with formulae $[Cu_2Ni_2L_2(py)_6]$ (**5**), $[Co_2Ni_2L_2(py)_6]$ (**6**), $[Co_2Cu_2L_2(py)_6]$ (**7**), $[Cu_2Zn_2L_2(py)_6]$ (**8**) and $[Ni_2Zn_2L_2(py)_6]$ (**9**) have been prepared and analyzed by SCXRD. Their composition has been established unambiguously. All complexes exhibit two weakly interacting [MM'] moieties, where some embody two level quantum systems. Compounds **5** and **8** each exhibit a pair of weakly coupled $S = ½$ spins that show quantum coherence in pulsed Q-band EPR, as required for quantum computing, with good phase memory times (T_M of 3.59 and 6.03 µs at 7 K). The reversible photo-switching of all the molecules is confirmed in solution. DFT calculations on **5** indicate that the interaction between both spins of the molecule can be switched ON and OFF upon photocyclization.

Introduction

Synthetic coordination chemistry is a useful tool for the design and preparation of molecular systems capable of realizing functional components of nanodevices.[1-3] Molecular spintronics aims to control the charge and the spin of electrons at the nanoscale, with the help of external stimuli.[4] These concepts apply to many scientific challenges such as the physical implementation of quantum computing.[5-6] This model of information processing depends upon the manipulation of coherent quantum states to encode information and a proposal has emerged recently for using the electronic spin carried by open-shell molecules to embody the quantum bits (qubits) and logic gates (qugates), opening fascinating challenges for synthetic chemistry.[7-11] Indeed, the two-level systems necessary for the implementation of qubits may consist of molecular entities with a true $S = ½$ isolated ground state,[12-14] or species exhibiting a magnetic doublet,[15-17] although exploiting two selected levels from a magnetic state with a multiplicity higher than two has also been studied.[18-19] In this context, an important goal is the preparation of molecules to model double (spin based) qubit quantum gates. Indeed 2qubit qugates will be necessary to construct any complex algorithm.[6, 20] Some quantum gates can be implemented by switching ON and OFF the magnetic interaction between both qubits.[21-22] It is conceivable that such control of the inter-qubit interaction within a molecular assembly could be triggered in an easy way using pulses of electromagnetic irradiation. Such a goal demands an effective synthetic design strategy in order to gather the required components in the appropriate disposition; these requirements are *i)* a pair of well-defined and weakly coupled spins and *ii)* a light-operated mechanism allowing reversible modification of the magnetic interaction between them. Here we propose to employ a diarylethene moiety as a photochromic switch (Scheme 1).

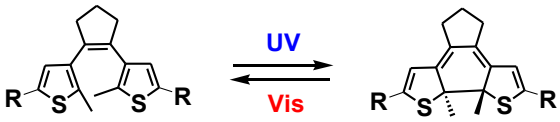

Scheme 1. Representation of a dithienylethene unit and its reversible photocyclization with UV and Visible light, respectively.

Diarylethenes represent a convenient choice as they possess many advantages;[23] *i*) they are amenable to extensive chemical functionalization, *ii*) they undergo reversible photocyclization with light of a different wavelength for each direction, *iii*) both isomeric forms are in most cases thermally stable, *iv*) the photochromic process is highly fatigue resistant and fast. Furthermore, as a promising precedent, the photo-switching of the electronic coupling between metal centres separated by this photochromic unit has been demonstrated using electrochemical techniques.[24-25] Some reports exist on the effect that the photo-isomerization of dithienylethene units have on the magnetic properties of transition metal complexes. The latter are connected to the photoactive unit through donor atoms

[a] Dr. J. Salinas Uber, Dr. M. Estrader, Dr. J. Garcia, P. Lloyd-Williams, A. Sadurní, Dr. G. Aromí
Departament de Química Inorgànica, Universitat de Barcelona, Diagonal 645, 08028, Barcelona, Spain. E-mail: guillem.aromi@qi.ub.es.
[b] D. Dengler, J. van Slageren
Physikalisches Institut, Universität Stuttgart, Pfaffenwaldring 57, 70550 Stuttgart, Germany.
[c] Dr. N. F. Chilton
School of Chemistry, The University of Manchester, Oxford Road, Manchester M13 9PL, United Kingdom.
[d] Dr. O. Roubeau
Instituto de Ciencia de Materiales de Aragón (ICMA), CSIC and Universidad de Zaragoza, Plaza San Francisco s/n, 50009, Zaragoza, Spain.
[e] Dr. S. J. Teat
Advanced Light Source, Berkeley Laboratory, 1 Cyclotron Road, Berkeley, California 94720, USA.
[f] Dr. J. Ribas-Ariño
Instituto de Ciencia de Materiales de Aragón (ICMA), CSIC and Universidad de Zaragoza, Plaza San Francisco s/n, 50009, Zaragoza, Spain.
[g] Dr. G. Aromí
Institute of Nanoscience and Nanotechnology (IN2UB) Universitat de Barcelona, Spain

incorporated into it, leading to mononuclear complexes,[26] coordination polymers of metals,[27-29] or cluster coordination polymers.[30-32] In the cases where slight modifications to the magnetic properties are observed upon photocyclization in the solid-state, these are due to changes in the crystal lattice in order to accommodate the structural rearrangement, and not to a switching of any through-bond magnetic interactions.

Here we present the design and preparation of a new dithienylethene photo-switchable ligand (H_4L, Scheme 2) separating a pair of 2-hydroxyphenyl-1,3-diketone units. The latter are designed to chelate and bridge two strongly coupled metal atoms, as a strategy to obtain molecular assemblies with [MM···MM] topology, incorporating a photochromic spacer. In this way, four homometallic complexes exhibiting the desired topology and formulated as $[M_4L_2(py)_6]$ (M = Cu, **1**; Co, **2**; Ni, **3**; Zn, **4**) have been prepared and studied in detail. Interestingly, the structural properties of the assembly enable the predetermined realization of site selective heterometallic architectures of the [MM'···M'M] type, allowing the design of a variety of spin pairs within the molecule. Thus, compounds $[Cu_2Ni_2L_2(py)_6]$ (**5**), $[Co_2Ni_2L_2(py)_6]$ (**6**), $[Co_2Cu_2L_2(py)_6]$ (**7**), $[Cu_2Zn_2L_2(py)_6]$ (**8**) and $[Ni_2Zn_2L_2(py)_6]$ (**9**) have been prepared and fully characterized. The combination of crystallographic analysis, density functional theory (DFT) calculations, metal microanalytical results and magnetic properties leave no doubts about the assignment of the metal distribution in all complexes. The reversible photo-switching properties of all the complexes have been probed spectroscopically in solution. Importantly, the quantum coherence of the most interesting architectures has been measured by pulsed EPR techniques. The effect of the photo-switching on the coupling between both spins of the molecule could be assessed through DFT calculations on complex **5**, indicating that the photo-cyclisation causes the switching of this interaction. The versatility shown by this family of molecules for choosing the identity of the spins, together with their addressability confirm that coordination chemistry represents a promising avenue to access sophisticated multifunctional molecules.

Results and Discussion

Synthesis

The new photochromic *bis*-β-diketone derivative H_4L was prepared through the functionalization of a *bis*-(thiophenyl)-cyclopentene as the active unit. The starting diarylethene comprises two peripheral carboxylate units (A, Scheme 2) and was synthesized according to an earlier reported procedure.[33] Subsequently, Steglich esterification[34] was carried out. As a result, 1,2-bis-(5-(2-acetylphenyl)-carboxylate-2-methylthiophen-3-yl)-cyclopentene (B) was obtained as a pure solid in excellent yield (over 90 %) after dry column chromatography. Double Baker-Venkataraman rearrangement[35] then furnished the final bis-β-diketone (Scheme 2). This reaction may be described as a (double) intramolecular Claisen condensation, carried out as a one-pot reaction in refluxing THF upon addition of a strong base (^{t}BuOK). Following this process, the aryloxy groups of both esters leave in the form of phenolates (Scheme 3).[36-38] The latter are protonated following an acidic work-up to yield the desired H_4L product. Its purification is carried out by recrystallization from acetone (60 % yield). The purity of this compound was established by microanalysis and ^{1}H-NMR (Fig S1), while its structure was determined by SCXRD (see below).

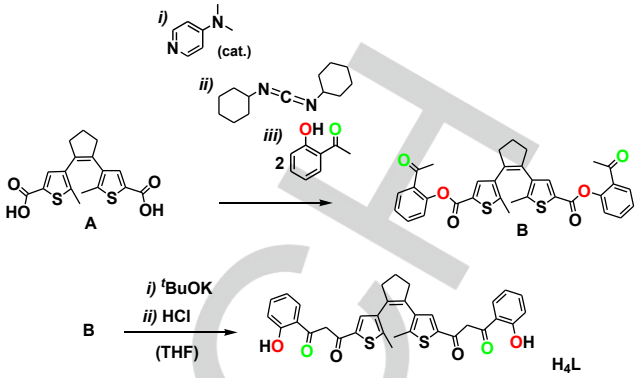

Scheme 2. Synthesis of H_4L.

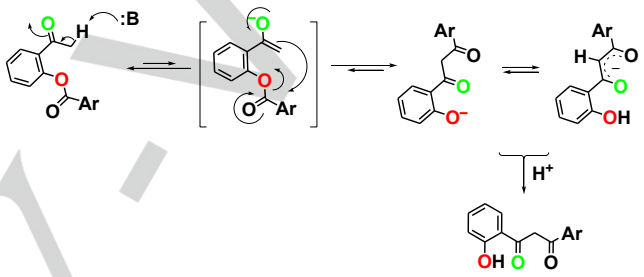

Scheme 3. Mechanism of the Baker-Venkataraman rearrangement as occurring in the formation of H_4L.

To the best of our knowledge, a double Baker-Venkataraman transposition has not been reported previously. This synthetic procedure provides access to a molecular entity incorporating photoactive spacers separating two 2-hydroxyphenyl/1,3-diketonato moieties, each capable of binding two coupled 3*d* metals.[39] Thus, H_4L has been designed for the preparation of molecules featuring two "independent" pairs of metal ions, as seen before,[40] now linked by a photochromic unit. Thus, reactions of H_4L under basic conditions with salts of Cu(II), Co(II), Ni(II) or Zn(II), respectively, produce crystals of the corresponding clusters with formulae $[M_4L_2(py)_6]$ (M=Cu, **1**; Co, **2**; Ni, **3**; Zn, **4**), exhibiting the predetermined [MM···MM] topology, as shown by SCXRD for all the compounds. The distinct coordination environment of the two types of metal sites present in the $[M_4]$ clusters (coordination numbers five and six, respectively; see below) suggests the possibility of accessing various types of heterometallic assemblies and of controlled composition and site selectivity. Thus, combining appropriate pairs of salts in equimolar amounts with stoichiometric quantities of H_4L and base afforded the heterometallic assemblies $[Cu_2Ni_2L_2(py)_6]$ (**5**), $[Co_2Ni_2L_2(py)_6]$ (**6**), $[Cu_2Co_2L_2(py)_6]$ (**7**), $[Cu_2Zn_2L_2(py)_6]$ (**8**) and $[Zn_2Ni_2L_2(py)_6]$ (**9**) in pure form, the structures of which could be established in detail by crystallography (see below). The metal contents were established by ICP, while the arrangement of these ions was predicted theoretically (see below) and corroborated through various physical techniques.

Description of the Molecular Structures

H_4L. This organic molecule crystallizes in the monoclinic space group *$P2_1/n$*. Crystallographic data are collected in Table S1. The asymmetric unit contains one molecule of H_4L and one of acetone. The structure confirms (Fig. 1) the formulation of the desired product, showing that it is present in the enolic form at either side. This tautomer is favoured by intramolecular hydrogen bonds (Fig. S2) and π-electron delocalization within the resulting moiety.[41] This configuration is also present in solution as shown by ^{1}H-NMR (Fig. S1). The π–system causes each 2-hydroxyphenyl-1,3-diketone group to lie approximately within one plane, shared by the neighbouring thiophenyl ring. Both idealized planes are kept at a mutual angle of 66.19°, through their connection to the central cyclopentene ring. This configuration also causes the methyl groups of the central photochromic spacer to exhibit the antiparallel conformation, keeping the C atoms that are to bind upon photocyclization (C13 and C21) 3.612 Å apart. This conformation and a C···C distance shorter than 4 Å are mandatory for observing the photoisomerization of the diarylethene unit in the solid state.[42] H_4L forms four fused triangular hydrogen bonds (Fig S2) via both of its 2-hydroxyphenyl-1,3-diketone units with the equivalent moieties from two other ligands, forming helical chains (Fig. S3), with both chiralities present in the lattice. Each ligand also establishes π···π stacking interactions *via* the 2-hydroxyphenyl-1,3-diketone conjugated systems with the counterpart from three other molecules, one on one side and two on the other, leading to stacks of four such fragments in the lattice (Fig. S4).

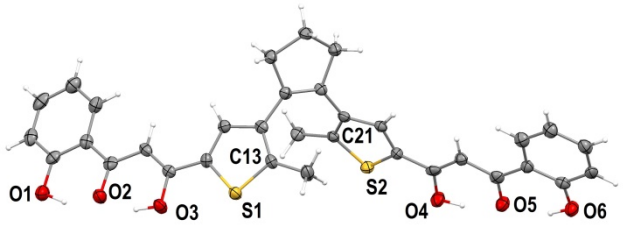

Figure 1. Partially labelled ORTEP representation of H_4L at 50% probability level. Hydrogen atoms are shown in white.

$[M_4L_2(py)_6]$ (M=Cu, 1; Co, 2; Ni, 3; Zn, 4). Complexes **1** to **4** are isostructural and crystallize in the orthorhombic space group *Pbca*. Crystallographic data are summarized in Table S1. Metric parameters are collected on Tables 1 and S3. The asymmetric unit is composed of one-half of the coordination cluster and 4.5 lattice molecules of pyridine (the fractional one lying in a special position). The unit cell incorporates eight such ensembles, thus four entire complex molecules. Since all the compounds are analogous, they will be described jointly. Molecules $[M_4L_2(py)_6]$ (Figs. 2 and S5 to S7) comprise two fully deprotonated H_4L ligands located face-to-face, holding four M(II) atoms disposed as a pair of separated dimers. The structure of H_4L fixes the position of the four metal ions in a [MM···MM] topology by occupying the equatorial coordination sites through their adjacent 1,3-diketonate and 2-hydroxybenzoketonate chelating moieties. In this manner, the M(II) centers remain closely connected pairwise through double monoatomic O-bridges. Molecules of pyridine occupy the axial positions. Interestingly, the metals at both ends of the cluster are five coordinate, in a square pyramidal geometry (τ = 0.08/0.27/0.07/0.17 in the **1**/**2**/**3**/**4** format, thus for Cu/Co/Ni/Zn)[43] whereas the internal metals have distorted octahedral coordination geometry. Such a combination of coordination geometries was previously observed on tetranuclear aggregates resulting from a related *bis*-*β*-diketonate.[40, 44] This occurrence was explained by the impossibility of the 2-hydroxybenzoketonate chelating moiety (more rigid than the 1,3-diketonate) to open up sufficiently and allow the metal to lie within a square equatorial environment, thus forcing instead a pyramidalization of this environment to expel the metal slightly outside of the square plane (here by 0.28/0.40/0.34/0.47 Å using again the **1**/**2**/**3**/**4** format).

This difference between both coordination pockets may be gauged by their O···O distances upon chelating (on average, 2.813 and 2.850 Å for **1**, 2.774 and 2.868 Å for **2**, 2.747 and 2.872 Å for **3**, and 2.807 and 2.893 Å for **4**, respectively). This pyramidalization would, presumably, prevent one of the axial ligands (the one opposite to the apex) to bind the metal. However, this may not be the only origin of the difference in coordination number. Indeed, inspection of the structure shows that the assembly seems to force a quite large angle, *θ*, between the equatorial planes of the adjacent sites (Fig. 3, *θ* = 23.44°/22.94°/20.97°/23.14°). This renders it impossible for both metals to be six coordinate due to steric encumbrance. The slight difference in chelating geometry of both pockets could in fact explain the precise location of the five and six coordination sites. Such combination of adjacent five and six coordination numbers is almost unique in the literature. In addition to the above mentioned tetranuclear clusters,[40, 44] it has been encountered on a related assembly involving *bis*-1,3,5-triketonates;[45] in this other system the adjacent equatorial planes form an angle of 10.88°, large enough to avoid the coordination of one of the four possible axial ligands. It thus features two distinct sites even if both chelating pockets are equal (1,3-diketonates). With simpler ligands comprising only two chelating rings, this effect disappears. Free of constraints from the rest of the structure, adjacent sites are both equal and octahedral.[46-49] In these cases, the equatorial planes are free to accommodate to the appropriate bond distances and lye parallel to each other, thus allowing the presence of the maximum number of axial ligands.

The above mentioned steric factors, causing discrimination into two different coordination numbers, offer a valuable and subtle synthetic tool; it can be exploited for the rational design of site selective heterometallic complexes with predetermined topologies by taking advantage of the coordination number preference of different 3d metals (see below).

The mean M–O bond distances in the 1/2/3/4 format are 1.945/2.012/1.977/2.035 (square pyramidal site) and 1.953/2.038/2.019/2.050 Å (octahedral site). Thus, in average, the octahedral sites have 0.4 to 2.1% longer equatorial bond distances than the five-coordinate sites, while the metals compared exhibit the following order of increasing bond distances; Cu<Ni<Co<Zn.

The free rotation about the C–C bond at the center of L4– leads to the overall “S” shape conformation of the assembly (Fig. S8). Within the aggregate, in all compounds the methylthiophenyl units of the photochromic moiety exhibit an antiparallel arrangement, with C···C separations of the photoactive carbon atoms of 3.604/3.562/3.583/3.581 Å. Therefore, in complexes 1, 2, 3 and 4, the structural requirements for the photocyclization are fulfilled. The molecular conformation causes both [M2]

dimers of the assembly to lie on two exactly parallel directions (Figs. 2 and S8) separated by 8.831/8.293/8.195/8.350 Å. Within the coupled dimers, the M···M distances are 3.053/3.189/3.042/3.284 Å, whereas the shortest inter-dimer, but intramolecular separations are 11.349/11.227/11.290/11.239 Å. In all cases, the complexes are held together through weak intermolecular interactions, mainly involving C–H···S, C–H···O or C–H···π contacts.

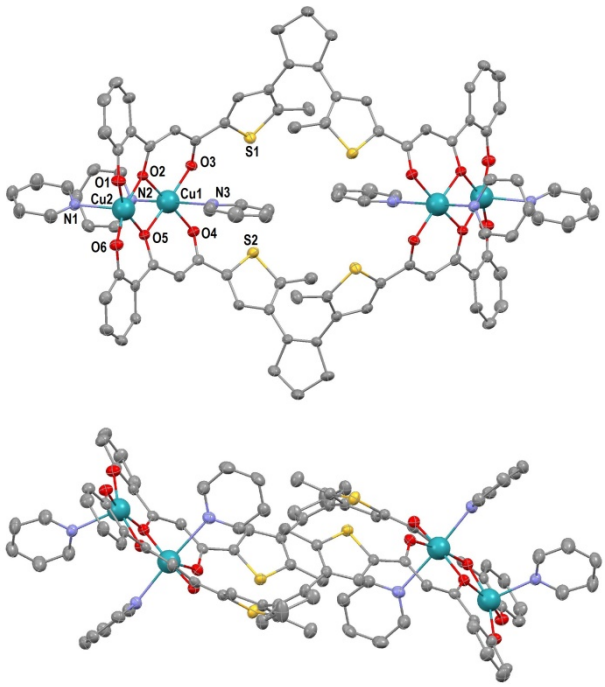

Figure 2. Two views of the ORTEP representation of $[Cu_4L_2(py)_6]$ (**1**) at 50% probability level (except the metals, represented as spheres), one of them partially labelled. Hydrogen atoms are not shown. Complexes $[Co_4L_2(py)_6]$ (**2**), $[Ni_4L_2(py)_6]$ (**3**) and $[Zn_4L_2(py)_6]$ (**4**) have the same molecular structure (See Figs. S5-S7).

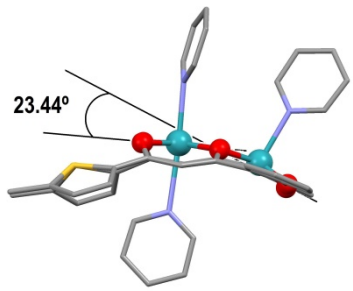

Figure 3. Representation of $[Cu_4L_2(py)_6]$ (**1**), emphasizing the angle between the equatorial planes of adjacent coordination sites (see text). The same pattern is observed in **2**, **3** and **4**.

$[M_2M'_2L_2(py)_6]$ (MM'=CuNi, 5; CoNi, 6; CuCo, 7; CuZn, 8; ZnNi, 9). Complexes **5** to **9** are isostructural with the homometallic analogues, therefore, much of the description has already been given above and is not repeated. Table 1 summarizes the crystallographic parameters and structural data are on Tables S2 and S3. Molecules $[M_2M'_2L_2(py)_6]$ (Fig. 4) also consist of two separate dimers of closely spaced metals, held together by laterally disposed L^{4-} ligands. The most interesting feature here is that there are two types of metals selectively distributed in the [MM'···M'M] topology, specifically [CuNi···NiCu] (**5**), [CoNi···NiCo] (**6**), [CuCo···CoCu] (**7**), [CuZn···ZnCu] (**8**) and [ZnNi···NiZn] (**9**), where the central positions are octahedral and the external ones are square pyramidal. The τ values of the five coordinate sites (τ = 0.06/0.23/0.08/0.09/0.14 for **5**/**6**/**7**/**8**/**9**, thus for metals Cu/Co/Cu/Cu/Zn) correlate well with these found for each of the metals in the homometallic counterparts, therefore supporting the observation of site selectivity (Fig. S9). Likewise, the separation of the metals from the basal plane, *d*, in these sites show the same correlation (0.29/0.41/0.28/0.33/0.47 Å for **5**/**6**/**7**/**8**/**9**, Fig. S9). Along the same lines, comparing the mean M–O bond distances in both geometries with the corresponding values in **1** to **4** also supports the position assignments of the various metals in the heterometallic molecules; these are 1.947/2.012/1.955/1.967/2.023 Å (square pyramidal, Fig. S10) and 2.011/2.011/2.028/2.019/2.008 Å (octahedral, Fig. S10) in the format **5**/**6**/**7**/**8**/**9**. Using the structures of the $[M_4L_2(py)_6]$ molecules to support the metal distribution in the heterometallic analogues is only ambiguous for [CuNi···NiCu] (**5**) since the parameters examined are very similar for both metals (Figs. S9 and S10). Other criteria, however, strongly support the identity of **5** (see below). In this series of molecules, the angle θ causing the dissymmetry in coordination numbers are 20.77°/22.90°/20.38°/22.21°/22.93°. Other metric parameters, not directly related to the heterometallic nature of these molecules are summarized in the caption of Fig. 4. From all the above observations, the distribution within the various [MM'···M'M] molecules presumably obeys the relative preference of the metals for occupying either a five- or a six-coordinate position, as dictated by the crystal field energy of each environment for each metal. The existence of complexes **1** to **4** shows that the four metals examined may occupy both sites. From the observations, Cu(II) has a marked tendency to be within a square pyramidal environment (except for one part in homometallic **1**, it is always seen in this position) whereas Ni(II) strongly prefers to be six-coordinate (always adopting this geometry, except when it is forced to be five-coordinate in **3**). Metals Co(II) and Zn(II) are seen to adapt their position to the preferred geometry of Cu(II) or Ni(II). Therefore, with Ni(II) these metals become square pyramidal (**6** and **9**) while they occupy the octahedral site when accompanied by Cu(II) (**7** and **8**). Interestingly, no product could be isolated from the reaction involving the combination Co/Zn.

Table 1. Structural parameters of complexes **1** to **9**, related to the metal distribution among both coordination sites.

	τ^a	d^b [Å]	$\langle d_{M\text{-}O}\rangle_{sp}{}^c$ [Å]	$\langle d_{M\text{-}O}\rangle_{oct}{}^d$ [Å]	Θ^e [deg]	dC21···C13$'$ [Å]
[CuCu], **1**	0.08	0.28	1.945	1.953	23.44	3.604
[CoCo], **2**	0.27	0.40	2.012	2.038	22.94	3.562
[NiNi], **3**	0.07	0.34	1.977	2.019	20.97	3.583
[ZnZn], **4**	0.17	0.47	2.035	2.050	23.14	3.581
[CuNi], **5**	0.06	0.29	1.947	2.011	20.77	3.559
[CoNi], **6**	0.23	0.41	2.012	2.011	22.90	3.571
[CuCo], **7**	0.08	0.28	1.955	2.028	20.38	3.573
[CuZn], **8**	0.09	0.33	1.967	2.019	22.21	3.590
[ZnNi], **9**	0.14	0.47	2.023	2.008	22.93	3.565

[a]Five-coordinate distortion parameter. [b]Metal distance to equatorial basal plane (square pyramidal site). [c]Equatorial average bond distances (square pyramidal site). [d]Equatorial average bond distances (octahedral site). [e]Angle between adjacent equatorial planes. [f] Distance between relevant C-atoms.

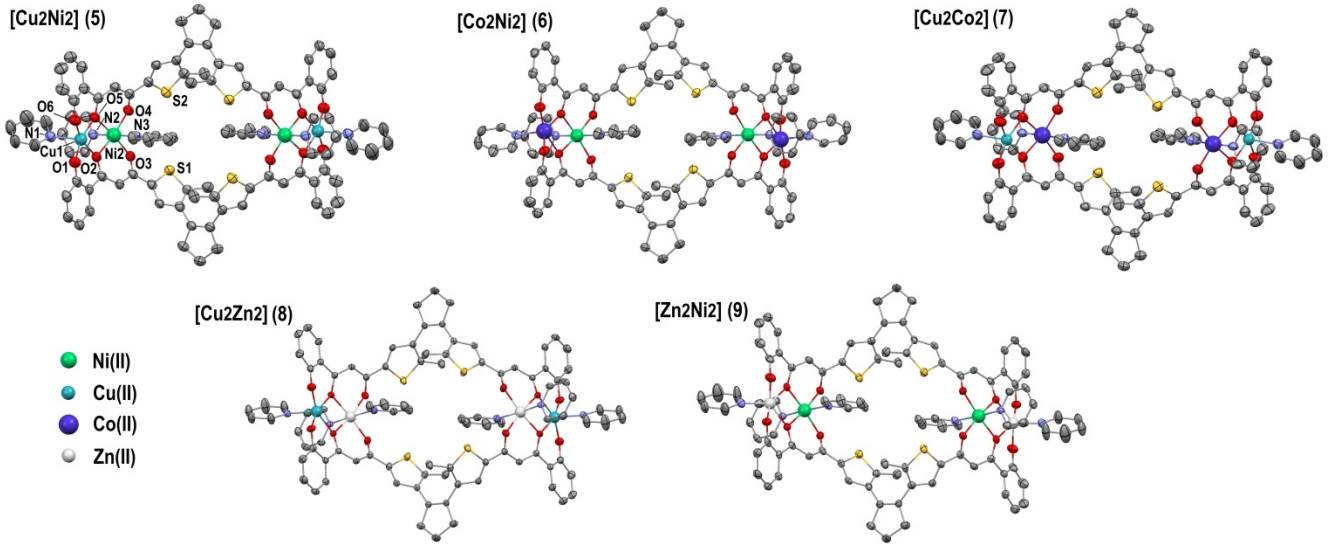

Figure 4. ORTEP representations of at 50% probability level level (except the metals, represented as spheres) of $[Cu_2Ni_2L_2(py)_6]$ (**5**), $[Co_2Ni_2L_2(py)_6]$ (**6**), $[Cu_2Co_2L_2(py)_6]$ (**7**), $[Cu_2Zn_2L_2(py)_6]$ (**8**) and $[Zn_2Ni_2L_2(py)_6]$ (**5**). Only unique heteroatoms and relevant C-atoms of **5** are labelled. The labelling is the same for the other molecules. Hydrogen atoms are not shown. Selected crystallographic parameters are (in the **5**/**6**/**7**/**8**/**9** format): Shortest intramolecular M···M' distances, 3.060/3.146/3.120/3.135/3.177 Å; second shortest intramolecular M···M distances, 11.166/11.280/11.120/11.204/11.233 Å; C13···C21, 3.559/3.571/3.573/3.590/3.565 Å; separation of the parallel M···M' (see text) directions, 8.295/8.197/8.411/8.602/8.074 Å.

DFT Calculations

DFT calculations were performed to support and quantify the efficiency of the site selectivity of ligand H_4L. The procedure was carried out for all the heterometallic systems described here. For this, the experimentally determined structure of the $[M_2M'_2L_2(py)_6]$ unit was employed for each of the compounds (**5**, **6**, **7**, **8** and **9**). The energy of the true metal distribution, [MM'···M'M] (A in Fig. 5), was compared to that of the other possible distributions; [M'M···M'M] (B), [M'M'···MM] (C) and [M'M···MM'] (D). The significance of the calculations using this procedure rely on the fact that the crystalline phases isolated were homogeneous and, very importantly, that all phases show 1:1 experimentally determined metal composition. In all cases, the DFT calculated relative energies (Table 2) were these of the high-spin configurations; this is not tremendously important since the smallest energy difference in Table 2 is one order of magnitude larger than the strongest magnetic coupling determined in these clusters (see below). The computed energies are in full agreement with the experimental results and are self-consistent; in all cases the energy cost of swapping two of the metal ions from their preferred locations (topologies B and C) is approximately one half the penalty of exchanging the positions of all metal ions (topology D) from the stable structure (topology A). These results imply that, all compounds exist virtually 100% in the Topology A configuration, and furthermore that Ni(II) and Cu(II) have the strongest preference for the six and five coordinate sites, respectively. Thus, Co(II) and Zn(II) are relegated to the remaining positions when they are in the presence of Cu(II) and Ni(II). We also observe that Co(II) shows a preference for being six coordinate, while Zn prefers to be five coordinate.

Table 2. Energies in cm^{-1} for the metal topologies in Figure 5 of complexes **5** to **9** as obtained through DFT calculations.

	Topology A	Topology B	Topology C	Topology D
[CuNi], **5**	0	7068	7132	14418
[CoNi], **6**	0	2505	2510	5559
[CuCo], **7**	0	5207	5303	10409
[CuZn], **8**	0	2839	3328	5674
[ZnNi], **9**	0	4009	4136	8030

Photo-switching Behaviour

The photo-switching behaviour of complexes **1** to **9** was investigated with UV-Vis spectroscopy on $5x10^{-5}$ M solutions in 1:1 toluene:DMSO (Figs. 6 and S11 to S19).

The absorption spectra of all the complexes are very similar; they feature one or two high energy π to π* transitions below 300 nm and one intense band, in some cases split or exhibiting shoulders, near 400 nm. The latter is attributed to metal-to-ligand charge transfer (MLCT) transitions, since it is also observed for complex $[Zn_4L_2(py)_6]$ (**4**). These bands are sufficiently intense so that the expected bands from *d-d* transitions cannot be seen in the same scale, except in $[Ni_4L_2(py)_6]$ (**3**), which features a very broad metal-based transition centred at 630 nm (Fig. 6). For all complexes, irradiation with UV light (λ < 425 nm) causes a reduction of the MLCT bands, in some cases accompanied by shifts and changes of shape and structure (Figs. 6 and S11 to S19). In addition, a very broad band grows gradually in the visible region while shifting slightly to higher energies. The maximum of this band at the photo-stationary state lies in the 620 to 651 nm range. This signal corresponds to the typical[50] π−π* transition within the polyenic system that forms upon photocyclization of the central diarylethene moieties of the complexes, which gives the strong coloration to the photo-generated compounds. In all cases, the various spectra cross at isosbestic points, indicating that the transformations are of zero order and only the initial and final products are present throughout the process. When the photo-stationary states are illuminated with visible light (λ > 430 nm) the band from the photochromic unit gradually decreases its intensity to finally disappear whereas the MLCT bands grow again. The disappearance of the former signal confirms that the photocyclization is reversed completely. The spectra recorded during the reverse process also feature isosbestic points, thus showing that the complexes do not disassemble during the transformation.

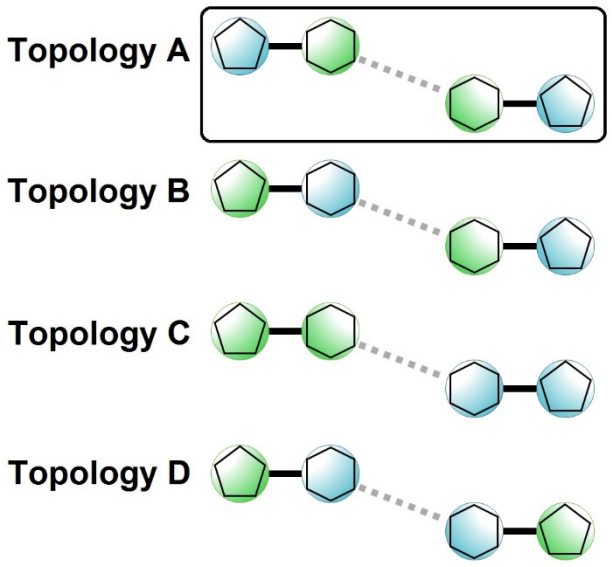

Figure 5. Metal topologies used for DFT calculations on complexes **5** to **9** using the coordinates from the structures obtained experimentally. The highlighted topology (top) corresponds to the one suggested by the experimental data, i.e. [CuNi···NiCu], [CoNi···NiCo], [CuCo···CoCu], [CuZn···ZnCu] and [ZnNi···NiZn], respectively.

The photo-isomerization in complexes $[Ni_4L_2(py)_6]$ (**3**, Figs. 6 and S13) and $[Co_4L_2(py)_6]$ (**2**, S12) is fully reversible. For the rest of the complexes, the reverse process takes place through a slightly ($[Co_2Ni_2L_2(py)_6]$ **6**, Fig. S16; $[Cu_2Zn_2L_2(py)_6]$ **8**, Fig. S18; $[Zn_2Ni_2L_2(py)_6]$ **9**, Fig. S19) or dramatically ($[Cu_4L_2(py)_6]$ **1**, Fig. S11; $[Zn_4L_2(py)_6]$ **4**, Fig. S14; $[Cu_2Ni_2L_2(py)_6]$ **5**, Fig. S15; $[Cu_2Co_2L_2(py)_6]$ **7**, Fig. S17) different pathway. Thus, the ring opening of the diarylethene moieties in these complexes yield slightly different species than the original ones. A plausible explanation is that the structural rearrangements occurring upon the photo-isomerization involve changes to the coordination geometries, and even to the number of pyridine ligands that are not reversed during the photo-induced ring opening. Complex $[Zn_4L_2(py)_6]$ (**4**) is the only one which does not recover the open form of its diarylethene moieties completely.

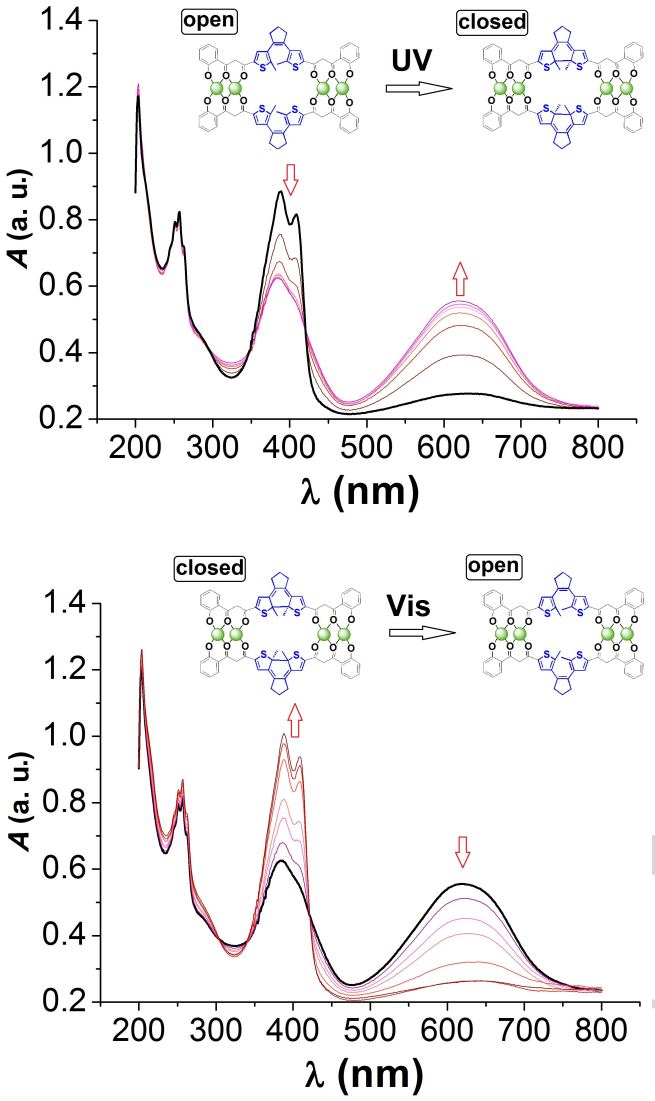

Figure 6. Top: Electronic absorption spectrum of $[Ni_4L_2(py)_6]$ (**3**) –bold line– in $5x10^{-5}$ M toluene/DMSO (1:1) solution and its evolution during irradiation with UV light (λ < 425 nm) over 2 min. Bottom: Electronic absorption spectrum of the above photo-converted product –bold line– and its evolution upon irradiation with visible light (λ > 430 nm) over 3 min.

Magnetic Properties

Variable temperature bulk magnetic susceptibility measurements were performed on polycrystalline samples of **1** – **3** and **5** – **9**. This served to confirm the metal composition of the complexes, especially the heterometallic ones, and to evaluate the strength and nature of intramolecular exchange interactions. The χT *vs.* T plots (χ is the molar paramagnetic susceptibility) of the homo- and hetereo-metallic compounds are given in the supplementary material, together with details of their analysis (Figs. S20-S23). Considering the singlet ground state resulting from the antiferromagnetic coupling in the homometallic systems, the ability to prepare complexes with two different metal ions at selected positions of the dinuclear moeties in complexes **5** to **9** is key to design molecular architectures with two well defined non-zero spin entities at the ground state. We focus here on the Cu/Ni systems to evaluate the potential of the photochromic assemblies as possible realizations of 2-qubit quantum gates.

Complexes $[Cu_2Zn_2L_2(py)_6]$ (**8**) and $[Zn_2Ni_2L_2(py)_6]$ (**9**) exhibit a nearly constant value of χT of 0.82/2.66 cm^3 K mol^{-1} (in the **8**/**9** format) over almost the entire temperature range, thus confirming the composition and the presence of isolated Cu(II)/Ni(II) ions in these complexes (expected values are 0.75/2 cm^3 K mol^{-1} for g = 2). Only at the lowest temperatures, a slight decrease of χT is observed, indicating departure from Curie's Law. In the case of **8**, this can only be ascribed to weak antiferromagnetic interactions, which could be either intra- and/or intermolecular (the Cu···Cu separation within the molecules is 1.60 nm). The data for **8** are equally-well reproduced using an intramolecular isotropic weak exchange interaction J = –0.24 and g = 2.08 or a Curie-Weiss model with C = 0.814 cm^3 K mol^{-1} and θ = –0.197 (Figs. 7, S21, see SI for details). The solid-state X-band EPR spectrum of $[Cu_2Zn_2L_2(py)_6]$ (**8**) is typical for an isolated copper(II) center with hyperfine split parallel transitions at low field and perpendicular transitions at higher fields, with g-values of $g_{||}$ = 2.307(2) and $g_{\perp}$ = 2.067(2) and hyperfine interactions of $A_{||}$ = 470(5) MHz and $A_{\perp}$ = 60(5) MHz, as derived from simulating it (Fig. 8). These values are typical for Cu(II) ions and in reasonable agreement with those derived from magnetic susceptibility. For **9**, the downturn of χT at low temperature necessarily involves the zero-field splitting of the Ni(II) ions, and the data are correctly reproduced with a ZFS term D_{Ni} = +4.56 or -9.95 cm^{-1} and g *ca.* 2.2 (see SI for details). The presence of a weak intramolecular antiferromagnetic interaction can however not be discarded given the shorter Ni···Ni separation (1.12 nm). It is expected to be smaller than that derived from fitting the data to a spin-only isotropic exchange, i.e. –0.54 cm^{-1} (Fig. S21). Similarly, the magnitude of D_{Ni} above should be considered as an upper ceiling.

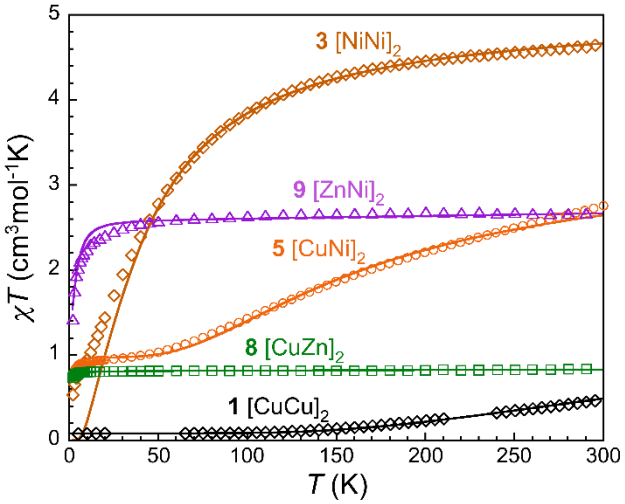

Figure 7. Plots of χT *vs.* T per mole of complexes **1** $[CuCu]_2$, **3** $[NiNi]_2$, **5** $[CuNi]_2$, **8** $[CuZn]_2$ and **9** $[ZnNi]_2$. The solid lines are fits of the experimental data (see text and SI for details).

The homometallic systems **1** and **3** exhibit a dominant antiferromagnetic coupling within each of their dinuclear entities (Figs. 7, S20). This interaction is particularly strong in complex $[Cu_4L_2(py)_6]$ (**1**), which exhibits a χT value at 300 K of 0.48 cm^3 K mol^{-1}, less than one third of the expected response for four uncoupled Cu(II) centers with g = 2 (expected, 1.5 cm^3 K mol^{-1}). A rapid decrease of χT occurs upon cooling to reach a steady value of *ca.* 0.06 cm^3 K mol^{-1} near 100 K (Figs. 7, S20).

The data is well-reproduced with an isotropic spin Hamiltonian H = $-2J\hat{\mathbf{S}}_1\cdot\hat{\mathbf{S}}_2$, where J is the coupling within the dinuclear entities of the complex.[51] A good fit was obtained without the need of any additional coupling constant,[52] yielding the parameters $J = -262$ cm^{-1}, $g = 2.10$ and a fraction of paramagnetic impurity of 2.5%. This coupling is similar to that seen on a related [CuCu···CuCu] complex exhibiting the same dinuclear moieties.[44] Such coupling through equatorial coordination bonds connected by alkoxide type atoms with Cu–O–Cu angles near 100° is expected.[53] The χT *vs.* T curve of $[Ni_4L_2(py)_6]$ (**3**, Figs. 7, S20) indicates a much weaker antiferromagnetic exchange, the values of 4.6-4.2 cm^3 K mol^{-1} down to about 150 K agreeing well with four uncoupled Ni(II) centres (expected 4.0 cm^3 K mol^{-1} for $g = 2$). A decrease of χT below 150 K may be attributed to the combined effects of the antiferromagnetic coupling within the Ni···Ni dinuclear sub-entities and the ZFS of the Ni(II) ions. The data are correctly reproduced (Figs. 7, S20) with $J = -12.0$ cm^{-1}, fixing g and D_{Ni} to the values derived for **8**, and considering a weak interaction between the central Ni(II) ions, fixed at the value derived for the [CuNi] analogue **5** (see below). This model significantly deviates from the experimental data in the low temperature region, where the experimental data do not tend to zero as expected. The most plausible origin of this discrepancy is the occurrence of not fully compensated spins within the antiferromagnetically-coupled Ni(II) pairs, possibly due to differing anisotropy axes at both Ni sites. This effect can be very strong in systems with large anisotropy and useful for building spin-based quantum gates as reported for a $[Tb_2]$ molecule.[54] Here, the outer pentacoordinated Ni(II) ion could be expected to exhibit a larger anisotropy than the central octahedral one, although we were unable to come to a reasonable model (see Fig. S20).

Complex $[Cu_2Ni_2L_2(py)_6]$ (**5**) exhibits a value of χT at 300 K of 3.46 cm^3 K mol^{-1}, above the calculated one for an uncoupled system and $g = 2$ (2.75 cm^3 K mol^{-1}), and showing already a decreasing trend with cooling, which suggests a moderate antiferromagnetic coupling and g values slightly above 2, as expected. The most remarkable feature of the χT *vs.* T plot (Figs. 7, S22) is the formation of a plateau near 50 K at ≈1.0 cm^3 K mol^{-1}, confirming the formation of a paramagnetic state within the [CuNi] entities over a large temperature range. A further decrease of χT below 10 K down to 0.76 cm^3 K mol^{-1} at 2 K can again be ascribed to intermolecular interactions between the exchange-coupled S = ½ moieties (since the analogous intramolecular coupling is expected to be very small, see below). The data are well-reproduced with $J_{Cu\cdots Ni}$ = -60 to -64 cm^{-1}, g_{Cu} = 2.20 and $J_{Ni\cdots Ni} = -0.2$ cm^{-1}, fixing g_{Ni} and D_{Ni} to the values derived for **8** (Fig. 7 and S22). In excellent agreement with this model, the X-Band EPR spectrum of a powder sample of **5** at 4 K shows a single line at $g = 2.22$ (Fig. 8), while the M *vs.* H plot at 2 K follows the Brillouin function calculated for two S = ½ and this same $g = 2.22$ (Fig. S22). The absence of noticeable anisotropy and hyperfine splitting of the EPR signal can be explained by the strong Cu-Ni exchange interaction, which dominates over the anisotropy of the Ni site alone as well as the hyperfine splitting of both Cu(II) and Ni(II). Note that the effective g value of the S = ½ ground state of each pair is largely determined by the g_{Ni}.[55] As for the [CuZn] moieties in **8**, there are, at this temperature, no signatures of intramolecular interaction between the [CuNi] exchange-coupled units in **5**, which is reasonable given the long M···M separation, 1.60 and 1.12 nm respectively for **8** and **5**. This agrees with the small $J_{Ni\cdots Ni}$ estimated above. This aspect is in fact particularly interesting, since such very weak interactions or inter-qubit separations are deemed appropriate for the development of spin-based 2-qubit quantum gates.[11, 16, 56] It is also important that at temperatures below 40 K, the excited quartet state is completely depopulated. Altogether, this renders the ground state of the [CuNi] (S = ½) moieties in **5** good definitions of qubits, as are naturally the isolated Cu(II) ions in the [CuZn] units in **8**.

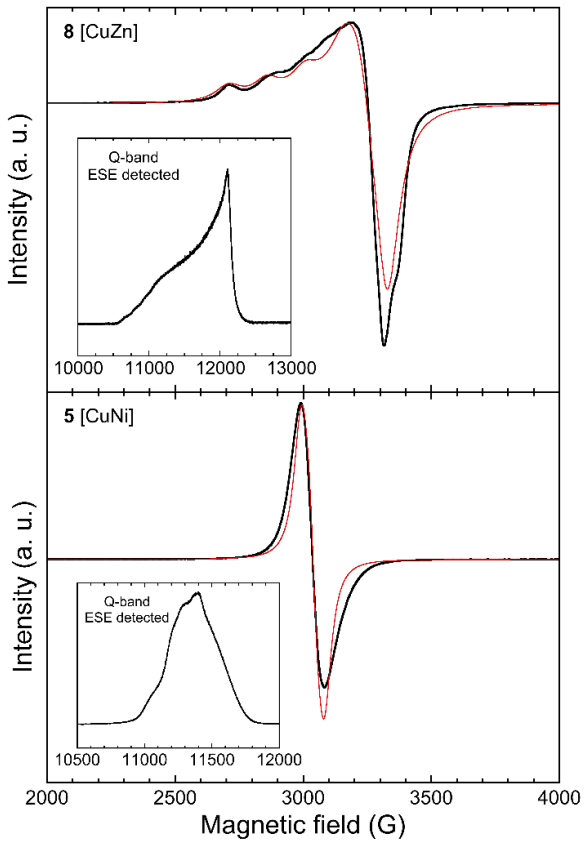

Figure 8. X-Band EPR spectra of powder samples of **8** [CuZn] (top) at 5 K and **5** ([CuNi] (bottom) at 4 K. The insets show the corresponding electron spin echo detected EPR spectra recorded on frozen solutions (toluene-d_8:dmso-d_6 1:1) at 35 GHz (Q-band) and 7 K.

A relevant property of any potential spin based qubit realization is its quantum coherence, which can be evaluated through pulsed Q-band EPR measurements. These were performed on both compounds **8** and **5** using dilute (1 mM) frozen solutions in toluene-d_8:dmso-d_6 (1:1). The dilute nature of the samples suppresses the detrimental effect of intermolecular electron spin interactions on the quantum coherence, whilst the deuteration of the solvent avoids the drawbacks from hyperfine interactions with solvent proton spins. Spectra detected via a Hahn echo sequence (insets in Fig. 8) are consistent with the CW powder spectra, proving the integrity of the species in solution. Inversion recovery and Hahn echo sequences were used to determine spin-lattice relaxation (T_1) and phase memory (T_M) times, respectively. All echo decay curves were found to be monoexponential and were analyzed as such (Fig. S24). Spin-relaxation times T_1 are of the same order for both compounds at

the lowest temperature (2.11(2) and 0.99(1) ms at 7 K, respectively; Fig. 9, Table S4). This reflects the similar chemical (geometrical structure) and physical (S = ½) nature of both. T_1 decreases more rapidly with increasing temperature for the [CuNi] qubits in **5** than for the [CuZn] ones in **8** (Fig. 9, Table S4). This and the overall longer T_1 for the latter can be explained by the presence of an excited S = 3/2 state for the former, which can function as the intermediate state in an Orbach-type relaxation process, thus opening up more relaxation pathways and shortening T_1. The phase memory time T_M for the [CuZn] spins in **8** is 6.03(1) µs at 7 K, which is reasonably long, especially considering the non-deuterated nature of the ligand and the axially ligated pyridine molecules. T_M decreases slowly with increasing temperature and above 50 K no reliable signal could be observed. At this temperature T_1 has decreased to a value close to T_M, thus becoming the limiting factor for the latter. The phase memory time for the [CuNi] qubits in **5** is T_M = 3.59(1) µs at 7 K, which is rather long for an exchange coupled system and in fact compares favourably with the previously reported exchange-coupled Cr_7Ni and Cu_3 qubits at similar temperatures.[57-58] Upon increasing the temperature, T_M diminishes despite T_1 still being consistently much longer than T_M. Such parallel decrease of T_1 and T_M was noted before.[59] The foregoing demonstrates that the S = ½ units in both $[Cu_2Zn_2L_2(py)_6]$ (**8**) and $[Cu_2Ni_2L_2(py)_6]$ (**5**) can embody qubits with reasonable coherence times. The combination of the very weak inter-qubit interaction at work and the possibility of affecting this interaction through irradiation makes these molecules suitable candidates for 2-qubit gate systems, and relevant measurements are now underway along this line. Unfortunately, full conversion of the photoactive group from the open to the closed form was so far not obtained in the solid-state, and therefore the effect of the photoconversion to the inter-qubit interaction could not be determined.

A quantitative description of the changes to the intramolecular spin-spin interaction upon photocyclization was obtained through DFT calculations on the [CuNi]···[NiCu] architecture (**5**). For these calculations, the geometry of the isolated molecule for each isomer was optimized (Fig S25). The computed energy spectra obtained for these geometries show that with the dithienylethene unit open, the inter-spin interaction is practically null (with an energy difference between the antiferromagnetic and the ferromagnetic states of 0.01 cm^{-1}). However, the closing of the ring that takes place upon irradiation with UV light switches the interaction ON, separating both states by 0.83 cm^{-1} (Fig. S26).

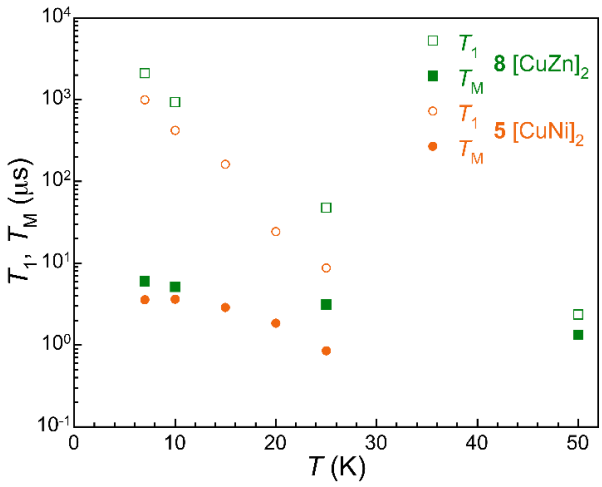

Figure 9. Spin-lattice relaxation (T_1, open symbols) and phase memory times (T_M, closed symbols) of toluene-d_8/dmso-d_6 1:1 frozen solutions of complexes **8** ([CuZn]$_2$, green symbols) and **5** ([CuNi]$_2$, orange symbols).

Conclusions

The Baker-Venkataraman transposition is proven to occur twice, in one reaction step, on two different positions of a molecule, as shown with the preparation of H_4L. This ligand leads to the formation of tetranuclear coordination complexes with a predetermined [MM···MM] topology (M= Cu, Co, Ni, Zn) exhibiting photo-switchable spacers between dinuclear metal aggregates. In this assembly, there are two chemically distinct sites featuring octahedral and square-pyramidal coordination geometries. This property allows pairs of different 3*d* metals to be discriminated by their coordination preferences and to prepare the pure heterometallic assemblies $[Cu_2Ni_2L_2(py)_6]$ (**5**), $[Co_2Ni_2L_2(py)_6]$ (**6**), $[Co_2Cu_2L_2(py)_6]$ (**7**), $[Cu_2Zn_2L_2(py)_6]$ (**8**) and $[Ni_2Zn_2L_2(py)_6]$ (**9**). From the ensemble of compounds, it becomes clear that Cu(II) and Ni(II) exhibit a strong preference for the square-pyramidal and the octahedral sites, respectively, while Co(II) and Zn(II) may occupy either of both sites depending on the nature of the metal with which they are paired. DFT calculations show that the metal topologies obtained experimentally are much more stable than any other distribution. This sophisticated supramolecular system has been designed as a potential model of spin-qased 2qubit quantum gates. All the heterometallic molecules (**5** to **9**) exhibit two well-defined, weakly interacting magnetic entities. The resonance between two magnetic levels of these units could be used as the implementation of a qubit. Particularly interesting are compounds **5** and **8**, which exhibit a pair of two level (S = ½) systems in the ground state. The resonance between these levels exhibits quantum coherence, which can be determined with pulsed EPR. The reversible photo-switching of the structure of all the molecules (except **4**, not fully reversible) was probed in solution through absorption spectroscopy. DFT calculations on complex **5** indicate that the reversible cyclization triggered by this photo-switching turns the interaction between the two spins of the molecule ON and OFF. These properties convert this family of coordination assemblies into promising functional devices, for example as models of light-operated 2-qubit quantum gates.

Experimental Section

Synthesis

The starting material 1,2-bis-(5-carboxy-2-methyl-thiophen-3-yl)-cyclopentene was synthesized according to a previously reported procedure.[33] All reagents were purchased from commercial sources and used as received. All coordination chemistry reactions were performed under aerobic conditions.

1,2-bis-(5-(3-oxo-3-(2-hydroxyphenyl)propanoyl)-2-methyl-thiophen-3-yl)-cyclopentene (H_4L). 1,2-bis-(5-carboxy-2-methyl-thiophen-3-yl)-cyclopentene (0.4 g, 1.15 mmol) and a catalytic amount (spatula tip) of 4-dimethylaminopyridine (DMAP) were dissolved in 10 mL of CH_2Cl_2 and 0.1 mL of dimethylformamide at 0°C. *N,N'*-dicyclohexylcarbodiimide (DCC, 0.711 g, 3.45 mmol) and 2'-hydroxyacetophenone (0.3 g, 2.53 mmol) were added and the mixture was allowed to warm to room temperature and was stirred for 12h. The resulting suspension was filtered and the filtrate washed with 1M aqueous $NaHCO_3$ (3 x 6mL) and H_2O (3 x 6 mL). The organic phase was dried with Na_2SO_4 and solvent removal led to a brown oil that was purified by column chromatography (silica gel with gradient elution of 1:9 EtOAc:hexane to 100% EtOAc). A pale brown solid corresponding to 1,2-bis-(5-(2-acetylphenyl)-carboxylate-2-methylthiophen-3-yl)-cyclopentene was obtained in a yield of 92.4 % (0.62 g). ^{1}H NMR (400 MHz, ppm, $CDCl_3$) 7.97-7.87 (m, 1H, ArH), 7.74 (s, 1H, $ArH_{thiophene}$), 7.70–7.61 (m, 1H, ArH), 7.42 (dd, *J* = 7.6, 1.1 Hz, 1H, ArH), 7.33 (dd, *J* = 8.1, 1.0 Hz, 1H, ArH), 2.84 (t, *J* = 7.5 Hz, 2H, CCH_2), 2.45 (s, 3H, $COCH_3$), 2.05 (s, 4H, CH_3+CH_2CH_2). HRMS (+ESI): *m/z* Calc. for [M-H]-$C_{33}H_{28}NaO_6S$: 607.1225. Found: 607.1219. Subsequently, this product (0.2 g, 0.349 mmol) was dissolved in anhydrous THF (10 mL) and a solution of ^{t}BuOK (0.87 mmol) was added. The resulting mixture was refluxed overnight under N_2. The slurry was allowed to cool to room temperature and filtered. The solid was left to dry and was then dissolved in 20 mL of H_2O. The solution was acidified to pH = 1 with concentrated HCl, leading to a yellow-greenish solid that was then filtered. The solid was purified by crystallization from acetone, affording yellow-green platelet crystals corresponding to H_4L in a yield of 60 % (0.11 g). Anal., found (calc% for $C_{31}H_{28}O_6S_2{\cdot}0.55C_3H_6O$; $H_4L{\cdot}0.55C_3H_6O$); C 66.17 (66.37), H 5.32 (5.5). ^{1}H NMR (400 MHz, ppm, $CDCl_3$) 15.69 (d, *J* = 19.3 Hz, 1H, OH_{enol}), 11.96 (d, *J* = 3.7 Hz, 1H, OH_{phenol}), 7.66 (dd, *J* = 8.1, 1.6 Hz, 1H , ArH), 7.49 (s, 1H, $CH_{thiophene}$), 7.42 (ddt, *J* = 11.3, 5.7, 2.8 Hz, 1H, ArH), 7.02–6.94 (m, 1H, ArH), 6.88 (qd, *J* = 6.9, 3.3 Hz, 1H, ArH), 6.52 (d, *J* = 4.4 Hz, 1H, CH_{enol}), 2.86 (t, *J* = 7.5 Hz, 2H, -CCH_2-), 2.15-2.10 (m, 1H, -$CH_2CH_2CH_2$-), 2.06–2.03 (m, 3H, CH_3). HRMS (+ESI): *m/z* Calc. for [M-H]-$C_{33}H_{29}O_6S$: 585.1406. Found: 585.1443.

$[Cu_4L_2(py)_6]$·9py (1·9py). A solution of H_4L (20 mg, 0.034 mmol) and 1M methanolic tetrabutylammonium hydroxide (TBAOH, 0.136 mL, 0.136 mmol) in pyridine (15 mL) was added to a solution of $CuBr_2$ (15.19 mg, 0.068 mmol) in pyridine (15 mL). The resulting dark orange mixture was stirred for 2 h, filtered and the solution was then layered with hexane. After one weak, orange crystals corresponding to the complex were collected (14 % yield, 11.5 mg). Anal., found (calc% for $C_{96}H_{78}Cu_4N_6O_{12}S_4{\cdot}2.65H_2O$; **1**·2.65$H_2O$); C 59.89 (59.57), H 4.11 (4.34), N 3.98 (4.34). IR (KBr pellet) v/cm^{-1}: 3439 b, 2917 w, 2847 w, 1600 m, 1500 s, 1443 s, 1365 m, 1326 m, 1247 m, 1195 m, 1130 m, 1030 w, 1000 w, 847 w, 791 w, 474 m, 700 w, 669 w, 573 w.

$[Co_4L_2(py)_6]$·9py (2·9py). A solution of H_4L (20 mg, 0.034 mmol) and 1M methanolic solution of TBAOH (0.136 mL, 0.136 mmol) in pyridine (15 mL) was added to a solution of $CoCl_2{\cdot}6H_2O$ (16.16 mg, 0.068 mmol) in pyridine (15 mL). The resulting dark orange mixture was stirred for 2 h, filtered and the solution then layered with ether. After one day, the complex was obtained as red crystals (10 % yield, 8.5 mg). Anal., found (calc% for $C_{96}H_{78}Co_4N_6O_{12}S_4{\cdot}2.3H_2O$; **2**·2.3$H_2O$); C 60.27 (60.26), H 4.39 (4.35), N 4.43 (4.40). The IR spectrum was identical to that of complex **1**.

$[Ni_4L_2(py)_6]$·9py (3·9py). A solution of H_4L (20 mg, 0.034 mmol) and 1M methanolic solution of TBAOH (0.136 mL, 0.136 mmol) in pyridine (15 mL) was added to a solution of $Ni(AcO)_2{\cdot}4H_2O$ (16.2 mg, 0.068 mmol) in pyridine (15 mL). The resulting dark orange mixture was stirred for 2 h, filtered and the solution then layered with ether. After three days, orange crystals were collected (13 % yield, 10.7 mg). Anal., found (calc% for $[C_{96}H_{78}Ni_4N_6O_{12}S_4]{\cdot}5H_2O$; **3**·5$H_2O$); C 58.91 (58.89), H 4.43 (4.53), N 4.13 (4.29). The IR spectrum was identical to that of complex **1**.

$[Zn_4L_2(py)_6]$·9py (4·9py). A solution of H_4L (20 mg, 0.034 mmol) and 1M methanolic solution of TBAOH (0.136 mL, 0.136 mmol) in pyridine (15 mL) was added to a solution of $Zn(AcO)_2$ (9.26 mg, 0.068 mmol) in pyridine (15 mL). The resulting dark orange mixture was stirred for 2 h, filtered and the solution then layered with hexane. After one weak, the complex was obtained as green crystals (13 % yield, 10.7 mg). Anal. % (CHN) Calc. (Found) for $[C_{86}H_{68}N_4O_{12}S_4Zn_4]{\cdot}8H_2O$; **4**(-2py)·8$H_2O$·: C 54.85 (54.61), H 4.50 (3.92), N 2.97 (2.63). The IR spectrum was identical to that of complex **1**.

$[Cu_2Ni_2L_2(py)_6]$·9py (5·9py). A solution of H_4L (20 mg, 0.034 mmol) and 1M methanolic solution of TBAOH (0.136 mL, 0.136 mmol) in pyridine (15 mL) was added to a solution of $Cu(NO_3)_2{\cdot}3H_2O$ (8.21 mg, 0.034 mmol) and $Ni(NO_3)_2{\cdot}3H_2O$ (9.88 mg, 0.034 mmol) in pyridine (15 mL). The resulting dark orange mixture was stirred for 2 h, filtered and the solution was then layered with hexane. After four days, orange crystals corresponding to the complex were obtained (16 % yield, 13.2 mg). Anal., found (calc% for $C_{86}H_{68}Cu_2Ni_2N_4O_{12}S_4{\cdot}6H_2O$; **5**·6$H_2O$–2py); C 56.34 (56.51), H 4.31 (4.41), N 2.88 (3.06). The IR spectrum was identical to that of complex **1**.

$[Co_2Ni_2L_2(py)_6]$·9py (6·9py). A solution of H_4L (20 mg, 0.034 mmol) and 1M methanolic solution of TBAOH (0.136 mL, 0.136 mmol) in pyridine (15 mL) was added to a solution of $Ni(AcO)_2{\cdot}4H_2O$ (8.71 mg, 0.035 mmol) and $Co(AcO)_2{\cdot}4H_2O$ (8.45 mg, 0.034 mmol) in pyridine (15 mL). The resulting dark orange mixture was stirred for 2 h, filtered and the solution was then layered with hexane. After four days, orange crystals were collected (12 % yield, 9.7 mg). Anal., found (calc% for $C_{96}H_{78}Co_2Ni_2N_6O_{12}S_4{\cdot}6H_2O$; **6**·6$H_2O$); C 58.57 (58.29), H 4.12 (4.59), N 3.75 (4.25). The IR spectrum was identical to that of complex **1**.

$[Cu_2Co_2L_2(py)_6]$·9py (7·9py). A solution of H_4L (20 mg, 0.034 mmol) and 1M methanolic solution of TBAOH (0.136 mL, 0.136 mmol) in pyridine (15 mL) was added to a solution of $Cu(AcO)H_2O$ (7.4 mg, 0.037 mmol) and $Co(AcO)_2{\cdot}4H_2O$ (8.46 mg, 0.034 mmol) in pyridine (15 mL). The resulting dark orange mixture was stirred for 2 h, filtered and the solution was then layered with ether. After one day, the complex was obtained as orange crystals (13 % yield, 11 mg). Anal., found (calc% for $C_{96}H_{78}Co_2Cu_2N_6O_{12}S_4{\cdot}1.65H_2O$; **7**·1.65$H_2O$); C 60.27 (60.38), H 4.32 (4.29), N 4.50 (4.40). The IR spectrum was identical to the one obtained for complex **1**.

$[Cu_2Zn_2L_2(py)_6]$·9py (8·9py). A solution of H_4L (20 mg, 0.034 mmol) and 1M methanolic solution of TBAOH (0.136 mL, 0.136 mmol) in pyridine (15 mL) was added to a solution of $CuCl_2{\cdot}2H_2O$ (5.78 mg, 0.034 mmol) and $ZnCl_2$ (4.62 mg, 0.034 mmol) in pyridine (15 mL). The resulting dark orange mixture was stirred for 2 h, filtered and the solution was then layered with hexane. After one day, orange crystals corresponding to the complex were collected (16 % yield, 13.4 mg). Anal., found (calc% for $C_{86}H_{68}Cu_2Zn_2N_4O_{12}S_4{\cdot}1.95H_2O$; **8**·2$H_2O$–3,75py); C 56.55 (56.94), H 3.76 (3.91), N 2.38 (1.94). The IR spectrum was identical to that of complex **1**.

$[Zn_2Ni_2L_2(py)_6]$·9py (9·9py). A solution of H_4L (20 mg, 0.034 mmol) and 1M methanolic solution of TBAOH (0.136 mL, 0.136 mmol) in pyridine (15 mL) was added to a solution of $NiCl_2{\cdot}6H_2O$ (8.08 mg, 0.034 mmol) and $ZnCl_2$ (4.62 mg, 0.034 mmol) in pyridine (15 mL). The resulting dark orange mixture was stirred for 2 h, filtered and the solution was then layered with ether. After one day, orange crystals were obtained (13 %

yield, 10.7 mg). Anal., found (calc% for $C_{86}H_{68}Ni_2Zn_2N_4O_{12}S_4 \cdot 5.2H_2O$; **9**·$6H_2O$–2.75py); C 55.69 (55.80), H 3.89 (4.34), N 2.98 (2.57). The IR spectrum was identical to that of complex **1**.

Physical measurements

Elemental analyses were performed with a Perkin-Elmer Series II CHNS/O Analyzer 2400, at the Servei de Microanàlisi of CSIC, Barcelona, Spain. IR spectra were recorded as KBr pellet samples on a Nicolet 5700 FTIR spectrometer. UV-Vis experiments were performed with a Varian Cary-100 spectrophotometer. ^{1}H-NMR spectra were recorded at room temperature with a Varian Unity 400 MHz spectrometer. ESI mass spectrometry was carried out using a LC/MSD-TOF spectrometer (Agilent Technologies) equipped with an electrospray ionization (ESI) source at the Serveis Cientificotècnics of the Universitat de Barcelona. Magnetic measurements were performed on polycrystalline samples with either a Quantum Design SQUID magnetometer MPMS-XL at the Physical Measurements Service of the Servicio de Apoyo a la Investigación-SAI, Universidad de Zaragoza, or a MPMS-5 magnetometer at the "Unitat de Mesures Magnètiques" of the Universitat de Barcelona. Analysis of metals were performed by inductively coupled plasma (ICP) spectrometry using a Varian Vista-MPX apparatus. X-Band EPR measurements were performed with a Bruker EMX spectrometer and pulsed Q-band measurements were performed on a custom-built spectrometer.[60] The pulse sequences used were π/2-τ-π-τ-echo (Hahn echo) for echo-detected EPR spectra and phase memory time determination and π-*T*- π/2-τ_{fix}-π-τ_{fix}-echo (inversion recovery) for spin-lattice relaxation time determination. Hahn echo decay curves were fitted to the expression $I = I_0 \exp(-2\tau/T_M)$ and inversion recovery decay curves to $I = I_0 (1-2\exp(-T/T_1))$ to extract the relevant decay time.

X-ray Crystallography

Data for H_4L, $[Cu_4L_2(py)_6]\cdot 9py$ (**1**·9py), $[Co_4L_2(py)_6]\cdot 9py$ (**2**·9py), $[Zn_4L_2(py)_6]\cdot 9py$ (**4**·9py), $[Co_2Cu_2L_2(py)_6]\cdot 9py$ (**7**·9py), $[Cu_2Zn_2L_2(py)_6]\cdot 9py$ (**8**·9py) and $[Ni_2Zn_2L_2(py)_6]\cdot 9py$ (**9**·9py) were collected using Mo Kα radiation (λ = 0.71073 Å) on a Bruker APEX II QUAZAR diffractometer equipped with a microfocus multilayer monochromator at 100 K. Data for $[Ni_4L_2(Py)_6]\cdot 9py$ (**3**·9py), $[Cu_2Ni_4L_2(Py)_6]\cdot 9Py$ (**5**·9py) and $[Co_2Ni_2L_2(Py)_6]\cdot 9py$ (**6**·9py) were collected on a Bruker APEX II CCD diffractometer at the Advanced Light Source beam-line 11.3.1 at Lawrence Berkeley National Laboratory, from a silicon 111 monochromator (λ = 0.7749 Å). Data reduction and absorption corrections were performed with SAINT and SADABS, respectively. All structures were solved and refined on F^2 with the SHELXTL suite,[61-62] and through the OLEX2 suite[63] for **1**, **2**, **4**, **7**, **8** and **9**. All non-hydrogen atoms were refined anisotropically. Due to some thermal disorder, a rather large number of atoms were refined with displacement parameters restraints, in particular, those of the pyridine moieties. Hydrogen atoms were placed geometrically on their carrier atoms and refined with a riding model. All details can be found in CCDC 1541350-1541359 (**H_4L**, **1**-**9**) that contain the supplementary crystallographic data for this paper. These data can be obtained free of charge from The Cambridge Crystallographic Data Center via https://www.ccdc.cam.ac.uk/structures/.

DFT Calculations

DFT calculations were carried out with the Gaussian 09 program using the B3LYP functional.[64] All single-point calculations were performed using an Ahlrichs TZVP basis set for all atoms.[65] For the geometry optimizations, the Ahlrichs SVP basis set was employed.[66]

Acknowledgements

G.A. thanks the Generalitat de Catalunya for the prize ICREA Academia 2008 and 2013 and the ERC for a Starting Grant (258060 FuncMolQIP). The authors thank the Spanish MINECO for funding through MAT2014-53961-R (OR) and CTQ2015-68370-P (GA) and the ERC for a Predoctoral Fellowship (JSU) under Grant 258060 FuncMolQIP. M.E. acknowledges the Spanish Ministry of Science and Innovation through the Juan de la Cierva Program. The Advanced Light Source (SJT) is supported by the Director, Office of Science, Office of Basic Energy Sciences of the U.S. Department of Energy under Contract DE-AC02-05CH11231.

Keywords: Lanthanides • Coordination Chemistry • Supramolecular Chemistry • DFT Calculations • Functional Molecules

[1] M. Castellano, R. Ruiz-García, J. Cano, J. Ferrando-Soria, E. Pardo, F. R. Fortea-Pérez, S.-E. Stiriba, W. P. Barros, H. O. Stumpf, L. Cañadillas-Delgado, J. Pasán, C. Ruiz-Pérez, G. de Munno, D. Armentano, Y. Journaux, F. Lloret, M. Julve, *Coord. Chem. Rev.* **2015**, *303*, 110-138.
[2] D. A. Shultz, M. L. Kirk, *Chem. Commun.* **2014**, *50*, 7401-7402.
[3] R. E. P. Winpenny, *Nat Nano* **2013**, *8*, 159-160.
[4] S. Sanvito, *Chem. Soc. Rev.* **2011**, *40*, 3336-3355.
[5] T. D. Ladd, F. Jelezko, R. Laflamme, Y. Nakamura, C. Monroe, J. L. O/'Brien, *Nature* **2010**, *464*, 45-53.
[6] M. A. Nielsen, I. L. Chuang, *Quantum Computation and Quantum Information*, Cambridge University Press, **2000**.
[7] A. Ardavan, S. J. Blundell, *J. Mater. Chem.* **2009**, *19*, 1754-1760.
[8] M. N. Leuenberger, D. Loss, *Nature* **2001**, *410*, 789-793.
[9] F. Meier, J. Levy, D. Loss, *Phys. Rev. Lett.* **2003**, *90*, 047901.
[10] R. E. P. Winpenny, *Angew. Chem., Int. Ed.* **2008**, *47*, 7992-7994.
[11] G. Aromi, D. Aguila, P. Gamez, F. Luis, O. Roubeau, *Chem. Soc. Rev.* **2012**, *41*, 537-546.
[12] G. A. Timco, T. B. Faust, F. Tuna, R. E. P. Winpenny, *Chem. Soc. Rev.* **2011**, *40*, 3067-3075.
[13] K. Bader, D. Dengler, S. Lenz, B. Endeward, S.-D. Jiang, P. Neugebauer, J. van Slageren, *Nat. Commun.* **2014**, *5*.
[14] J. M. Zadrozny, J. Niklas, O. G. Poluektov, D. E. Freedman, *J. Am. Chem. Soc.* **2014**, *136*, 15841-15844.
[15] J. J. Baldoví, S. Cardona-Serra, J. M. Clemente-Juan, E. Coronado, A. Gaita-Ariño, A. Palii, *Inorg. Chem.* **2012**, *51*, 12565-12574.
[16] D. Aguilà, L. A. Barrios, V. Velasco, O. Roubeau, A. Repollés, P. J. Alonso, J. Sesé, S. J. Teat, F. Luis, G. Aromí, *J. Am. Chem. Soc.* **2014**, *136*, 14215-14222.
[17] K. S. Pedersen, A.-M. Ariciu, S. McAdams, H. Weihe, J. Bendix, F. Tuna, S. Piligkos, *J. Am. Chem. Soc.* **2016**, *138*, 5801-5804.
[18] M. S. Fataftah, J. M. Zadrozny, S. C. Coste, M. J. Graham, D. M. Rogers, D. E. Freedman, *J. Am. Chem. Soc.* **2016**, *138*, 1344-1348.
[19] M. J. Martinez-Perez, S. Cardona-Serra, C. Schlegel, F. Moro, P. J. Alonso, H. Prima-Garcia, J. M. Clemente-Juan, M. Evangelisti, A. Gaita-Arino, J. Sese, J. van Slageren, E. Coronado, F. Luis, *Phys. Rev. Lett.* **2012**, *108*.
[20] A. Barenco, C. H. Bennett, R. Cleve, D. P. DiVincenzo, N. Margolus, P. Shor, T. Sleator, J. A. Smolin, H. Weinfurter, *Phys. Rev. A* **1995**, *52*, 3457-3467.
[21] J. Lehmann, A. Gaita-Ariño, E. Coronado, D. Loss, *Nat. Nanotechnol.* **2007**, *2*, 312-317.
[22] S. Cardona-Serra, J. M. Clemente-Juan, A. Gaita-Arino, N. Suaud, O. Svoboda, E. Coronado, *Chem. Commun.* **2013**, *49*, 9621-9623.
[23] M. Irie, *Chem. Rev.* **2000**, *100*, 1685-1716.
[24] K. Motoyama, T. Koike, M. Akita, *Chem. Commun.* **2008**, 5812-5814.
[25] Y. Tanaka, A. Inagaki, M. Akita, *Chem. Commun.* **2007**, 1169-1171.
[26] N. Z. K. Sénéchal-David, M. Walko, E. Halza, E. Rivière, R. Guillot, B. L. Feringa, and M.-L. Boillot, *Dalt. Trans.* **2008**, 1932-1936.

[27] M. M. J. Han, Y. Suenaga, H. Ebisu, A. Nabei, T. Kuroda-Sowa, and M. Munakata, *Inorg. Chem.* **2007**, *46*, 3313-3321.

[28] J. H. M. Munakata, M. Maekawa, Y. Suenaga, T. Kuroda-Sowa, A. Nabei, and H. Ebisu, *Inorg. Chim. Acta* **2007**, *360*, 2792-2796.

[29] J. S. Uber, M. Estrader, C. Mathoniere, R. Clerac, O. Roubeau, G. Aromí, *Cryst. Growth Des.* **2016**, *16*, 4026-4033.

[30] M. Morimoto, H. Miyasaka, M. Yamashita, M. Irie, *J. Am. Chem. Soc.* **2009**, *131*, 9823-9835.

[31] M. R. D. Pinkowicz, L.-M. Zheng, S. Sato, M. Hasegawa, M. Morimoto, M. Irie, B. K. Breedlove, G. Cosquer, K. Katoh, and M. Yamashita, *Chem., Eur. J.* **2014**, *20*, 12502-12513.

[32] H. M. S. Takuya, M. Yamashita, M. Morimoto, and M. Irie, *Dalt. Trans.* **2011**, *40*, 2275-2282.

[33] J. J. D. d. J. L. N. Lucas, J. H. van Esch, R. M. Kellogg, and B. L. Feringa, *Eur. J. Org. Chem.* **2003**, 155-166.

[34] B. Neises, W. Steglich, *Angew. Chem., Int. Ed.* **1978**, *17*, 522-524.

[35] D. Ameen, T. J. Snape, *Synthesis* **2015**, *47*, 141-158.

[36] W. Baker, *J. Chem. Soc.* **1933**, 1381-1389.

[37] D. C. Bhalla, H. S. Mahal, K. Venkataraman, *J. Chem. Soc.* **1935**, 868-870.

[38] H. S. Mahal, K. Venkataraman, *J. Chem. Soc.* **1934**, 1767-1769.

[39] G. Aromi, P. C. Berzal, P. Gamez, O. Roubeau, H. Kooijman, A. L. Spek, W. L. Driessen, J. Reedijk, *Angew. Chem., Int. Ed.* **2001**, *40*, 3444-3446.

[40] L. A. Barrios, D. Aguila, S. Mellat, O. Roubeau, S. J. Teat, P. Gamez, G. Aromi, *C. R. Chim.* **2008**, *11*, 1117-1120.

[41] G. Aromi, P. Gamez, C. Boldron, H. Kooijman, A. L. Spek, J. Reedijk, *Eur. J. Inorg. Chem.* **2006**, 1940-1944.

[42] S. Kobatake, K. Uchida, E. Tsuchida, M. Irie, *Chem. Commun.* **2002**, 2804-2805.

[43] A. W. Addison, T. N. Rao, J. Reedijk, J. Vanrijn, G. C. Verschoor, *J. Chem. Soc., Dalton Trans.* **1984**, 1349-1356.

[44] L. A. Barrios, D. Aguila, O. Roubeau, P. Gamez, J. Ribas-Arino, S. J. Teat, G. Aromi, *Chem., Eur. J.* **2009**, *15*, 11235-11243.

[45] F. Li, J. K. Clegg, P. Jensen, K. Fisher, L. F. Lindoy, G. V. Meehan, B. Moubaraki, K. S. Murray, *Angew. Chem., Int. Ed.* **2009**, *48*, 7059-7063.

[46] J. M. Kuszaj, B. Tomlonovic, D. P. Murtha, R. L. Lintvedt, M. D. Glick, *Inorg. Chem.* **1973**, *12*, 1297-1303.

[47] J. W. Guthrie, R. L. Lintvedt, M. D. Glick, *Inorg. Chem.* **1980**, *19*, 2949-2956.

[48] P. Boyd, K. Lee, M. Zvagulis, *Aust. J. Chem.* **1986**, *39*, 1249-1256.

[49] R. L. Lintvedt, L. L. Borer, D. P. Murtha, J. M. Kuszaj, M. D. Glick, *Inorg. Chem.* **1974**, *13*, 18-26.

[50] S. Kobatake, M. Irie, *Bull. Chem. Soc. Jpn.* **2004**, *77*, 195-210.

[51] B. Bleaney, K. D. Bowers, *Proc. R. Soc. London Ser. A* **1952**, *214*, 451-465.

[52] P. E. Kruger, G. D. Fallon, B. Moubaraki, K. S. Murray, *J. Chem. Soc., Chem. Commun.* **1992**, 1726-1729.

[53] G. Aromi, J. Ribas, P. Gamez, O. Roubeau, H. Kooijman, A. L. Spek, S. Teat, E. MacLean, H. Stoeckli-Evans, J. Reedijk, *Chem., Eur. J.* **2004**, *10*, 6476-6488.

[54] F. Luis, A. Repolles, M. J. Martinez-Perez, D. Aguila, O. Roubeau, D. Zueco, P. J. Alonso, M. Evangelisti, A. Camon, J. Sese, L. A. Barrios, G. Aromi, *Phys. Rev. Lett.* **2011**, *107*.

[55] A. Bencini, D. Gatteschi, *EPR of exchange coupled systems*, Springer-Verlag, Berlin, **1990**.

[56] J. Ferrando-Soria, E. Moreno Pineda, A. Chiesa, A. Fernandez, S. A. Magee, S. Carretta, P. Santini, I. J. Vitorica-Yrezabal, F. Tuna, G. A. Timco, E. J. L. McInnes, R. E. P. Winpenny, *Nat. Commun.* **2016**, *7*, 11377.

[57] C. J. Wedge, G. A. Timco, E. T. Spielberg, R. E. George, F. Tuna, S. Rigby, E. J. L. McInnes, R. E. P. Winpenny, S. J. Blundell, A. Ardavan, *Phys. Rev. Lett.* **2012**, *108*, 107204.

[58] P. Lutz, R. Marx, D. Dengler, A. Kromer, J. van Slageren, *Mol. Phys.* **2013**, *111*, 2897-2902.

[59] C. Schlegel, J. van Slageren, M. Manoli, E. K. Brechin, M. Dressel, *Phys. Rev. Lett.* **2008**, *101*, 147203.

[60] I. Tkach, A. Baldansuren, E. Kalabukhova, S. Lukin, A. Sitnikov, A. Tsvir, M. Ischenko, Y. Rosentzweig, E. Roduner, *Appl. Magn. Reson.* **2008**, *35*, 95-112.

[61] G. M. Sheldrick, *Acta Cryst., Sect. A* **2008**, *64*, 112-122.

[62] G. M. Sheldrick, *Acta Cryst. A* **2015**, *71*, 3-8.

[63] O. V. Dolomanov, L. J. Bourhis, R. J. Gildea, J. A. K. Howard, H. Puschmann, *J. Appl. Crystallogr.* **2009**, *42*, 339-341.

[64] A. D. Becke, *J. Chem. Phys.* **1993**, *98*, 5648-5652.

[65] A. Schäfer, C. Huber, R. Ahlrichs, *J. Chem. Phys.* **1994**, *100*, 5829-5835.

[66] A. Schäfer, H. Horn, R. Ahlrichs, *J. Chem. Phys.* **1992**, *97*, 2571-2577.

FULL PAPER

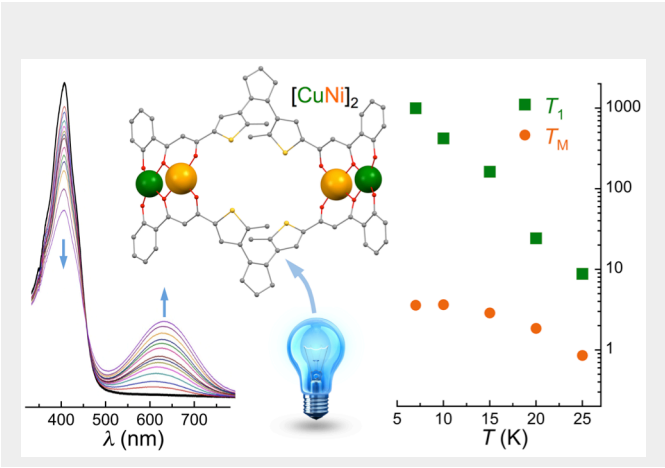

J. Salinas Uber, M. Estrader, J. Garcia, P. Lloyd-Williams, A. Sadurní, D. Dengler, J. van Slageren, N. F. Chilton, O. Roubeau S. J. Teat, J. Ribas-Ariño, G. Aromí**

Page No. – Page No.

Molecules Designed to Contain Two Weakly Coupled Spins with a Photo-switchable Spacer